



# Parametric Dynamic Simulation and Bayesian Design Optimization of a Front-Loading Washing Machine

Fatemeh Hashemian<sup>1</sup> · Haizhou Yang<sup>2</sup> · Yi Wang<sup>1</sup> · Xiaomin Deng<sup>1</sup> · Seungoh Kim<sup>3</sup> · Raveendran Vaidhyanathan<sup>4</sup>

Received: 23 September 2023 / Revised: 16 March 2024 / Accepted: 22 April 2024  
© The Author(s) 2024

## Abstract

**Objective** This paper presents the dynamic modeling and design optimization of a fully parametrized front-loading washing machine.

**Methods** A thorough mathematical analysis is performed to capture the effect of nine design variables (including rotation speed, spring stiffness, weight balancer mass density, damping coefficient, spring and damper angles) on vibrational characteristics of the washing machine. The parametric simulation reveals a complex relationship between the vibrational dynamics and design variables, entailing a computationally efficient optimization approach. A Bayesian Optimization (BO) framework is developed, in which a Gaussian process model and Genetic Algorithm (GA) are utilized along with carefully selected acquisition functions to enable adaptive sampling and search for optimal design values. The objective function is to minimize the maximum amplitude of the tub displacement inside the washing machine body. Two case studies are performed to consider a different number of design variables and choices of various infill methods.

**Results** Results show that the fully parametrized front-loading washing machine model is applicable for parametric simulation and design optimization. The proposed BO is able to successfully find a set of design variable values corresponding to the lowest maximum displacement for vibration reduction. A comparison analysis is also carried out to exhibit the difference in optimization convergence and computational cost caused by the choice of acquisition functions.

**Conclusion** It is shown that the fully parametrized washing machine model yields a lower maximum displacement than the model with fewer design variables. Of the two acquisition functions studied for optimization, the Expected Improvement function converges more rapidly than the Lower Bound criterion.

**Keywords** Washing machine · Bayesian optimization · Genetic algorithm · Acquisition functions · Adaptive sampling

## Introduction

It has been many years since home appliances with vibration behavior, such as washing machines, became an important field of study for researchers [1–3] to improve energy efficiency [4] and stability and noise reduction [5]. One serious

issue that needs to be studied is the vibration-induced walking problem that occurs when the machine operates at a high speed [5, 6], which is a stability concern, produces large noise, and leads to poor energy efficiency. Another one is the collision of internal components of the washing machine during its operation, which needs to be avoided [7]. Therefore, a more stable, quiet, and light weighted washing machine is desired by customers [1]. As such, design optimization of the washing machine comes to the scene with the benefit of keeping a balance between energy consumption and stability.

So far, two major types of washing machines have been investigated, including front-loading (with a horizontal rotation axis) [3] and top-loading (with a vertical rotation axis) [8]. Due to its popularity in use, front-loading washing machines are the focus of the current study. It should be noted that a majority of front-loading washing machine

✉ Yi Wang  
yiwang@cec.sc.edu

<sup>1</sup> Department of Mechanical Engineering, University of South Carolina, Columbia, SC 29208, USA

<sup>2</sup> Department of Mechanical Engineering, University of Michigan, Ann Arbor, MI 48109, USA

<sup>3</sup> Digital Appliance Division, Advanced R&D, Suwon, Republic of Korea

<sup>4</sup> Digital Appliance ATO SAMSUNG ELECTRONICS CO., LTD, Pine Brook, NJ, USA

studies have been conducted to develop active, passive, or hybrid approaches to reduce undesired motion caused by the unbalanced force generated by the unevenly distributed mass while the machine is in operation [3]. In order to address these issues, it is important to perform dynamic modeling and understand the most critical parameters affecting the vibration and dynamic behavior of the washing machine.

There are numerous research efforts of investigating the dynamic performance and vibration reduction of washing machines. Jo et al. [9] developed a robotic balancer that quantifies unbalance mass and phase angle during the washing machine spin cycle of a front-loading drum-type washing machine. The balancer actively produces an opposing force due to laundry and water dropping that occur during the washing process that proactively rebalances the system. Jang et al. [10] established a multibody dynamic model of a vertical axis washing machine to analyze the vibration of a washing machine during the dehydration process using a method called rapid decrease of the unbalanced liquid mass. Then, the vibration of the multibody dynamic model during the dehydration process with a rapid decrease of unbalanced liquid mass was analyzed to reduce the vibrations. Yalçın and Erol [11] developed a semiactive vibration control method to improve the dynamic stability of a horizontal axis washing machine by adjusting the maximum force produced by the semiactive suspension elements.

In the context of the dynamic performance of the washing machines, researchers also investigated the effect of using automatic or hydraulic balancers. Chen et al. [12] developed an active balancing system using water as a counteract to suppress vibrations in a vertical axis washing machine. They created a dynamic model to design a control system that displaces water to counteract unbalanced laundry loads, then manufactured and tested an equipped washing machine prototype with this active balancing mechanism. Hong and Chen [13] studied the dynamic performance of a drum-type washing machine by establishing a detailed dynamic model with an automatic counter-balancing model of balls. Chen et al. [14] built a mathematical model of a horizontal-axis washing machine with a ball balancer and carried out a stability analysis to study the stable and unstable regions. Another solution to the issue of vibration reduction is to study the effect of important parameters influencing the washing machine suspension system or to conduct a sensitivity analysis [15]. Park et al. [16] developed a linear dynamic model for front-loading washing machines to identify important parameters and critical parameter ranges for modeling.

Many researchers have also developed optimization algorithms for washing machine suspension systems along with dynamic modeling and parametric studies. Xiao and Zhang [17] proposed dynamics analysis and parameter optimization of a drum washing machine based on the rigid-flexible coupling technology of virtual prototypes. Furthermore, a

sensitivity analysis was conducted to enhance the optimization of two key parameters: spring stiffness and damping coefficient. Nygård and Berbyuk [18] proposed a multiobjective optimization formulation and a sensitivity analysis to address the vibration issues caused by unevenly distributed loads. The vibration resulting from unevenly distributed load was considered in the cost function for optimization to assess tub motion performance, prevent collisions, minimize transmitted forces, and improve stability. Boyraz and Gündüz [1] introduced a method employing genetic algorithms (GA) to optimize vibration characteristics of a horizontal-axis washing machines, alongside a novel measurement technique capable of determining both 2D displacement and vibration frequency from acceleration data. While their study combined passive and active methods for reducing vibration in washing machines, their approach utilized a 2D dynamic model and an optimization of six parameters, including spring stiffness, damping coefficient, and the  $x$  and  $z$  coordinates of springs and dampers. Chen and Zhang carried out a full factorial experiment design of a horizontal axis washing machine with a ball balancer to investigate the importance of six different parameters. Then, they constructed a cubic polynomial regression model and performed a parametric optimization using a hybrid scheme to search the optimal parameter values [2]. However, their algorithm was used for the optimization of six parameters. In et al. [19] investigated the variability in spin time and spin vibration of washing machines, attributing it to uncertainty in unbalanced mass caused by the position or shape of laundry inside the drum during the spin process. Additionally, they improved the washing machines' performance by optimizing the spin algorithm. However, the focus of their study was only on the spin algorithm.

In the previous effort [20], a thorough study on the effects of various design variables on the dynamic behavior and vibration characteristics of a front-loading washing machine was conducted analyzing a set of nine critical design variables using the commercial multibody simulation software Adams View. In addition, a sensitivity analysis was conducted to examine how changes in these design variables affect both the natural frequency and overall dynamic performance of the front-loading washing machine. It is worth noting that while there are valuable studies conducted on the dynamic behavior of washing machines, there remains a need for comprehensive research that considers a thorough list of design parameters affecting the washing machine suspension behavior and achieve salient performance of vibration reduction through computationally efficient optimization.

Within this context, the focus of the present effort is to develop new and comprehensive numerical models with a large number of design variables to investigate the vibrational characteristics of front-load washing machines

through numerical simulations and optimization. This study is devoted to addressing the need for design optimization with the following contributions. First, a new washing machine dynamics model including nine design variables is developed to analyze the vibrational characteristics, and the mathematical relationship between each design variable and system dynamics is derived through meticulous geometrical analyses. Second, the dynamic model is utilized in a parametric analysis to manifest the complex vibrational behavior and its dependence on design variables. Lastly, a Bayesian Optimization is performed to minimize the maximum displacement response of the front-loading washing machine. Bayesian Optimization is chosen over other optimization algorithms since it is a highly sample-efficient method for searching global optimum, that is, it can find better solution while running faster with a relatively smaller number of function evaluations [21]. The comparison of the optimization results using a different number of design variables convincingly confirms that simultaneously optimizing a larger set of design variables allows more room for vibration mitigation and yields better performance. The choice of the acquisition functions in Bayesian Optimization leads to different convergence rate and computational cost of optimization. To our knowledge, the development of vibration models and investigation of the vibrational characteristics for a front-loading washing machine, characterized by nine design variables and optimized using Bayesian optimization to attain the optimal solution, marks a substantial enhancement over prior research endeavors.

This paper is organized as follows. The problem formulation is presented in Sect. “[Problem Description](#)”, which introduces the objective function and design variables of the optimization problem. Sect. “[Methodology](#)” elucidates

the proposed Bayesian Optimization framework, including the derivation of nine design variables, the Gaussian Process model, Genetic Algorithm (GA), and adaptive sampling. In Sect. “[Result and Discussion](#)”, the results of Bayesian Optimization with various infill criteria for two case studies are discussed. Finally, this study concludes with a summary in Sect. “[Conclusion](#)”.

## Problem Description

The solid model of the washing machine studied in this paper is designed in a CAD, and then the multibody dynamics simulation of the model is performed using the Adams View, as shown in Fig. 1. The dynamic system of the front-loading washing machine contains a motor, a tub, a drum, front and rear weight balancers, two springs attached to the top of the tub, and four dampers linked to the tub’s lower portion (see Sect. “[Design Variable Definition](#)” for more details). The washing machine is composed of ten movable bodies, including a drum body, a tub body, and a piston and cylinder for each of the four dampers. The washing machine frame is considered to be the reference ground. Both the drum and tub are treated as rigid bodies, with their deformation effect neglected. Additionally, the left and right springs are symmetric with respect to the Y–Z plane, and the front and rear dampers located at the left and right sides of the washing machine are perfectly symmetrical with respect to the Y–Z plane.

In the present study, a Bayesian Optimization is performed to minimize the maximum displacement amplitude of the tub to avoid any potential collision. To capture

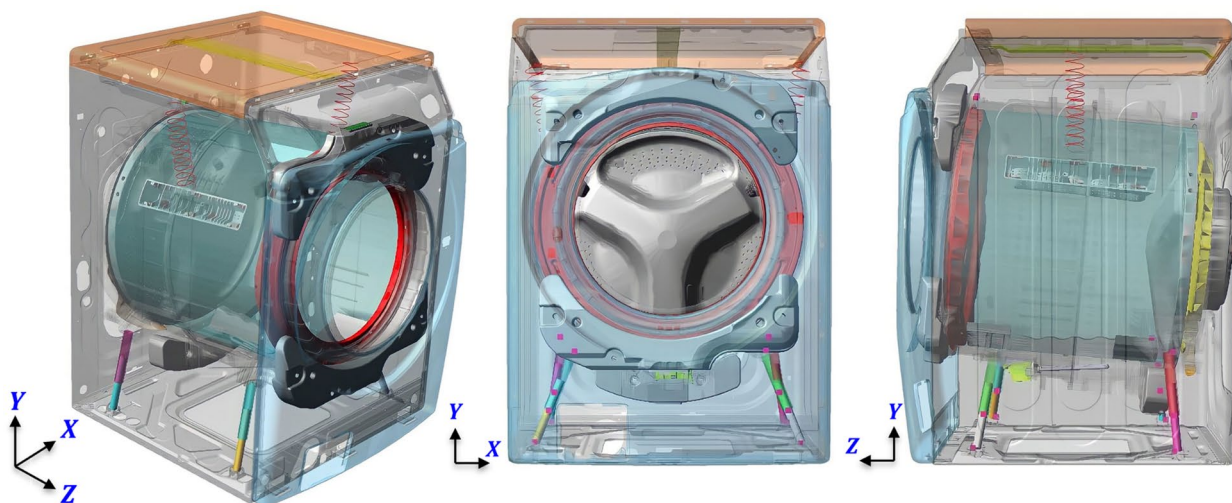


Fig. 1 A front-loading washing machine created in Adams View

the tub's displacement response, the response data of the maximum displacement amplitude of the front top sensor attached to the tub in the washer model is investigated in this paper. The objective function of this optimization problem is described as

$$x^* = \min_{x \in R^d} f(x) \quad (1)$$

where  $f$  is the displacement of the tub,  $x \in R^d$  represents design variables, including the rotation speed, spring stiffness, spring angle, weight balancer mass density, damper coefficient, and location and orientation of the dampers, and  $d$  is the number of design variables, which is 9 in this paper. All the design variables will be introduced in Sect. "Dynamic Simulation" and elaborated more in Sect. "Design Variable Definition". Typically, optimization based on dynamic simulation is computationally demanding due to a large number of objective function evaluations. Therefore, a Bayesian Optimization algorithm is used to accelerate the optimization, which utilizes the underlying Gaussian Process model, i.e.  $f_{GP}(x)$  to judiciously select the locations within the parameter space for the next round of simulation, i.e., adaptive infill, that balances between exploration and exploitation.

## Methodology

As seen in Fig. 2, a Bayesian Optimization (BO) framework with an adaptive infill sampling is proposed to minimize the displacement of the tub, which includes several steps: initial sampling, data generation, model construction, and adaptive sampling. BO has exhibited a superior performance compared to other optimization algorithms [22]. It is a remarkably efficient method well suited for global optimization where other methods such as gradient-based optimization might struggle in cases where objective function might have multiple local optima [21]. For an overview of BO, please see Wang et al. [22]. The detailed procedure is given as follows: initially, a multi-dimensional hypercube of the parameter space is defined, which includes all the design variables along with their lower and upper bounds, i.e., Block (1) in Fig. 2 (detailed in Sect. "Design Variable Definition"). Then, Latin hypercube sampling (LHS) is performed to generate initial samples [23] to fill the parameter space for the dynamic simulations, i.e., Block (2) in Fig. 2. Numerical simulations of the washing machine are carried out at these samples, i.e., Block (3) in Fig. 2 to generate the initial training data set for modeling, i.e., Block (4) in Fig. 2. In this work, the data is the maximum displacement amplitude extracted from a dynamic simulation. Then, the samples and the generated training data set are used as the input–output data pairs to construct a Gaussian process regression (GPR) model, capturing the relationship between design parameters and maximum displacement amplitude as shown in Block (5) in Fig. 2. Since the initial GPR model is not sufficiently

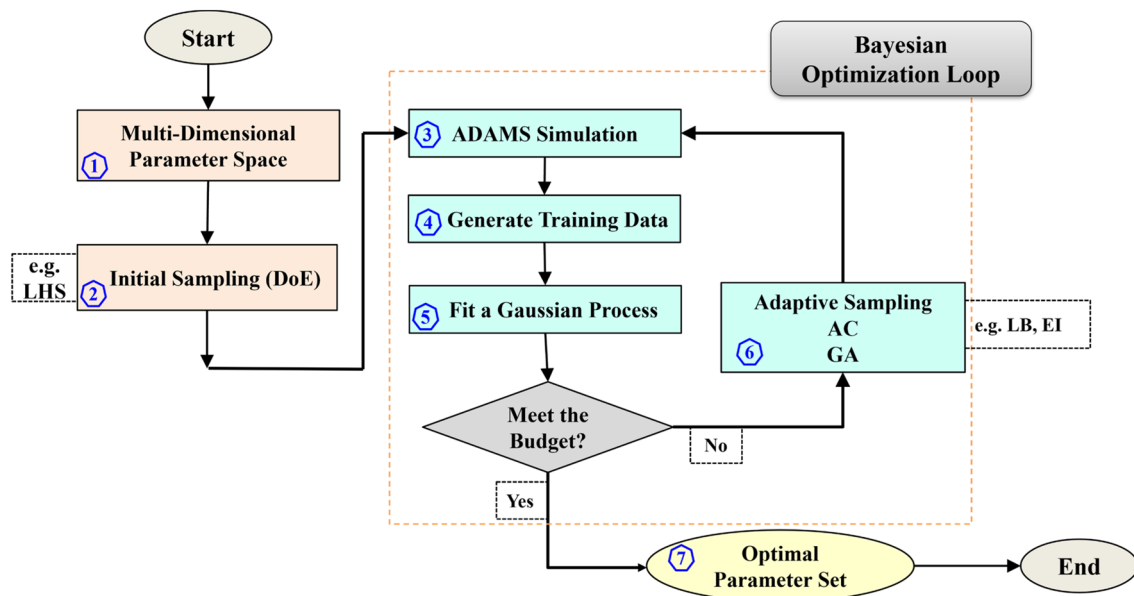


Fig. 2 BO flowchart with adaptive sampling for the front-loading washing machine



accurate to cover the design space or search for the global optimum, an adaptive sampling process is incorporated into the framework to add new samples to the data set and update the model iteratively. A genetic algorithm is utilized to optimize the acquisition functions (that is abbreviated as 'AC' in Fig. 2) given the infill criteria for locating the infill location, i.e., Block (6) in Fig. 2. In this study, two different infill criteria are examined for adaptive sampling, and their convergence performances are compared. Then, the infill sample is supplied to ADAMS simulation to produce new training data, and the new data is subsequently added to the existing training data set to update the model. This process will be repeated iteratively until the maximum number of iterations is reached. Finally, the optimal parameter set found by the proposed framework is the design for the washing machine, which produces the minimum displacement amplitude, i.e., Block (7) in Fig. 2.

### Dynamic Simulation

In order to analyze the behavior of the washing machine and generate the training data, Adams View is used to perform numerical simulations. Each simulation evaluates a dynamic process for 120 s, during which the drum's rotation speed increases monotonically from zero at the beginning of the washer operation to a given rotation speed DV\_W defined as the maximum speed during steady-state operation. DV\_W is entered by the user prior to each simulation, as shown in Fig. 3.

In order to prevent collisions between the washing machine's tub or other internal components and the washer frame, it is essential to minimize the vibration amplitude of the tub. Achieving this requires a thorough evaluation of the washing machine's suspension system and a concerted effort

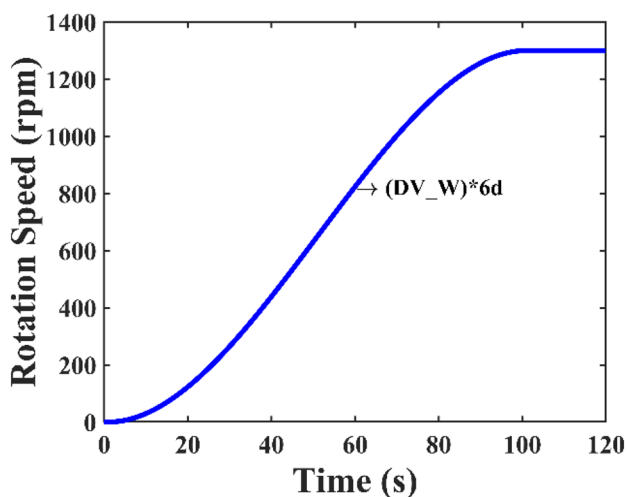


**Fig. 3** The variation of the washing machine drum rotation speed with time

among various design variables. While one might initially consider increasing the distance between the tub and frame as a solution, altering the size of the tub or the frame is not feasible due to conflicts with standard washing machine specifications, extra costs, and additional space requirements for installation.

### Design Variable Definition

Before the analysis, our model needs to be built as a function of possible design variables/parameters influencing the vibration of the washing machine. Therefore, model parameterization is one of the most important parts of the study. A full structure of the front-loading washing machine is presented in Fig. 4. A list of nine independent design variables (DVs) are used to describe the washer model in Adams View and investigate their geometrical effects on vibration characteristics. The standard values (the nominal or default values) of these DVs in the washer model are presented in Table 1.

### Spring Stiffness and Spring Angle

The spring stiffness is an input parameter in Adams View and is chosen as the design variable DV\_K in this study. However, the parameterization of the spring angle is more complicated than it seems. The left and right spring locations (when the washer is stationary) are aligned with the mass center of the entire tub-drum assembly, and thus, the upper and lower end points of both springs lie in the vertical plane that is parallel to the X–Y plane (see Fig. 5) and pass through the mass center. To satisfy this requirement, the Z coordinates of the end points of both springs are set equal to  $Z_{mc}$ , the Z coordinate of the mass center of the entire tub-drum assembly. The spring angle is set to be the same for both the left and right springs. Each spring has two ends: the end connected to the washing machine frame is named marker  $i$ , and the end connected to the tub is named marker  $j$ . For both springs, the marker  $j$  position during design is located on an elliptic curve formed by the intersection of the plane  $Z = Z_{mc}$  and the tilted cylindrical surface of the tub, whose radius is determined by the distance from the  $j$  marker to the axis of rotation of the tub-drum assembly. Also, the line connecting the shaft mass center at the back of the washing machine to the mass center of the drum-front component at the front will be most aligned with the axis of rotation of the tub-drum assembly. The tilt angle  $\theta$  of the axis of rotation, from the back of the tub to the front of the tub, is approximately  $5^\circ$ .

Using the shaft mass center location as a reference point, which is represented as  $(X_0, Y_0, Z_0) = (0, 51.4888, 71.9637)$  (mm) and the tilt angle  $\theta = 5^\circ$ , the following expressions for

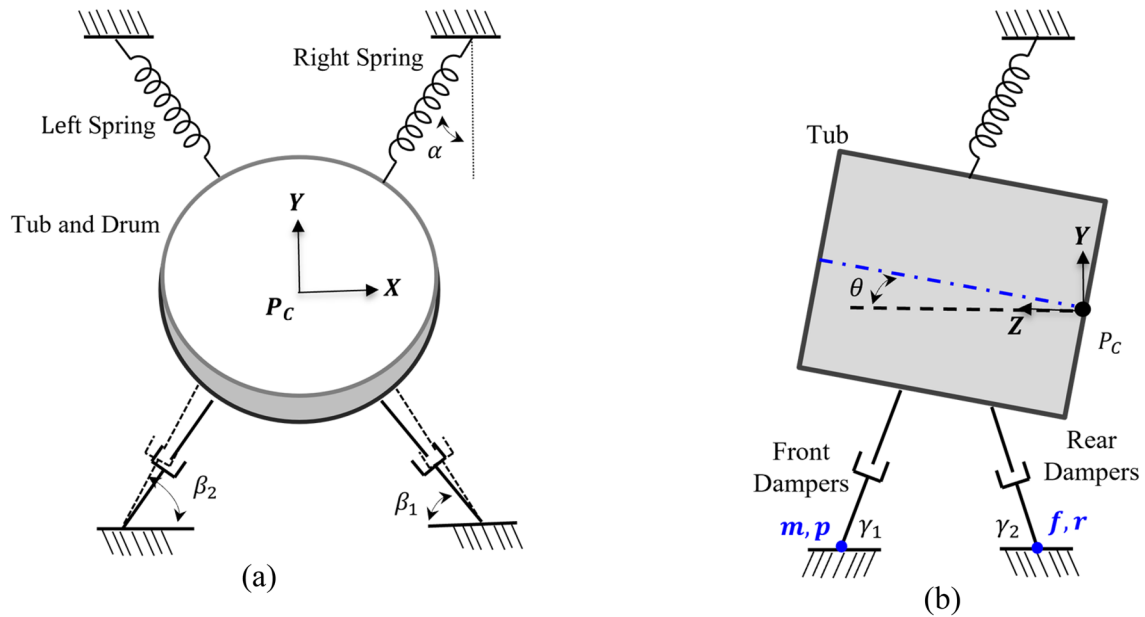


**Fig. 4** (a) A front-loading washing machine created in Adams View with schematic drawings (left and right) showing the spring angle  $\alpha$ , the front dampers' front angle  $\beta_1$  and the rear dampers' front angle  $\beta_2$ , and (b) schematic drawings of the front damper side angle  $\gamma_1$  and the rear dampers' side angle  $\gamma_2$

**Table 1** Nine design variables with their upper and lower bounds and standard values implemented in the Adams View dynamics model for the washing machine

Parameters	Symbol	Unit	Nominal value	Lower Limit	Upper Limit
Rotation speed (DV_W)	W	rpm	1300.00	800.00	1700.00
Spring stiffness (DV_K)	K	kgf/mm	1.20	0.65	1.75
Spring Angle (DV_A)	A	°	12.87	5.00	18.00
Weight balancer mass density (DV_MD)	m	kg/mm <sup>3</sup>	4.50E-06	4.07E-06	9.37E-06
Damping Coefficient (DV_C)	C	kgf.s/mm	0.50	0.00	1.50
Front damper front angle (DV_FA)	$\beta_1$	°	68.28	65.50	71.50
Rear damper front angle (DV_RA)	$\beta_2$	°	80.96	77.90	84.40
Front damper side angle (DV_DFR)	$\gamma_1$	°	80.24	70.25	90.22
Rear damper side angle (DV_DRR)	$\gamma_2$	°	84.95	74.95	94.95

the marker  $j$  location ( $X_j, Y_j, Z_{mc}$ ) are given in Eqs. (2a), (2b), (3), and (4) below

$$X_j = X_i + (Y_i - Y_j) \tan \alpha \tag{2a}$$

$$Y_j = \frac{b + \sqrt{b^2 - ac}}{a} \tag{2b}$$

where Eq. (2a) relate the global X and Y coordinates of marker  $j$  to the spring angle  $\alpha$  as shown in Fig. 5. These two

coordinates defined in Eq. (2a) and Eq. (2b) are obtained considering the conditions that markers'  $j$  moves along the elliptic curve formed by the intersection of the plane  $Z = Z_{mc}$  and the tilted cylindrical surface of the tub. The variation of the X and Y coordinates of marker  $j$  along the elliptic curve will result in the variation of spring angle  $\alpha$ . Intermediate variables are introduced to simplify equation expression and progressive derivations, and all these variables are given in Eqs. (3) and (4)

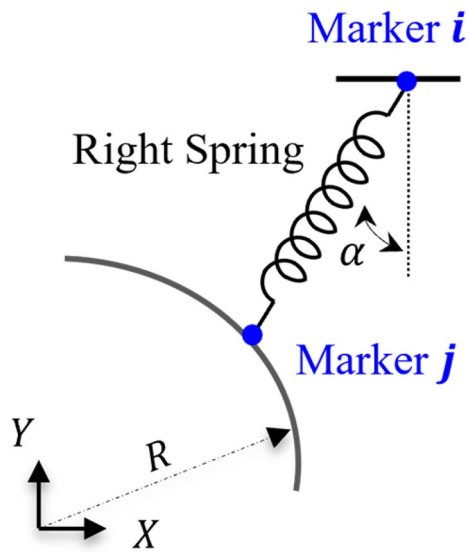


Fig. 5 The schematic drawings (on the right side) showing the spring angle ( $\alpha$ ) and end points  $i$  and  $j$

$$\begin{aligned}
 a &= a_1^2 + a_2^2, \\
 b &= a_1 b_1 + a_2 b_2, \\
 c &= b_1^2 + b_2^2 - R^2,
 \end{aligned}
 \tag{3}$$

$$\begin{aligned}
 a_1 &= \pm \tan \alpha, \\
 a_2 &= \cos \theta, \\
 b_1 &= X_i \pm Y_i \tan \alpha, \\
 b_2 &= Y_0 \cos \theta + (Z_{mc} - Z_0) \sin \theta
 \end{aligned}
 \tag{4}$$

In Eq. (4), the sign + is for the left spring, and - is for the right spring. The radius  $R$  of the cylindrical surface, on which the spring marker  $j$  is attached, is the distance from the marker to the tilted axis of rotation and is given a value of  $R = 329.27$  mm. The expressions in Eqs. (2a), (2b), (3), and (4) are implemented in the Adams model, not as a design variable, but as a function expression to calculate automatically the marker  $j$  locations for the left and right springs when the design variable  $DV\_A$  for the spring angle  $\alpha$  is changed during design optimization.

**Weight Balancer Mass Density**

The design variable  $DV\_MD$  for the mass density ( $\rho_f$ ) of the front-up and -down weight balancers (see Fig. 1) is added to the model with a nominal value of  $4.50E-06$  (kg/mm<sup>3</sup>). The maximum value for  $DV\_MD$  is the one when the mass of a weight balancer is increased by 10 kg while keeping the volume unchanged (that is, the geometry of the weight balancer is unchanged). The mass density parameter is designed in a way that when the mass density of the front weight balancers is varied, that of the rear weight balancer will be modified

accordingly. Then, the  $Z$  coordinate of the mass center of the entire tub-drum assembly (consisting of 32 parts) remains the same, that is  $Z_{mc} = 334.562675$  (mm). According to this requirement, the following expression is derived in Eq. (5) relating the density of the rear weight balancer,  $\rho_r$ , to that of the front weight balancer,  $\rho_f$  :

$$\rho_r = \frac{[(Z_{mcN} - Z_{mc})M_N + (Z_{mcfu} - Z_{mc})\rho_f V_{fu} + (Z_{mefd} - Z_{mc})\rho_f V_{fd}]}{(Z_{mc} - Z_{mcr})V_r}
 \tag{5}$$

where,  $Z_{mcN}$  and  $M_N$  are, respectively, the  $Z$  coordinate of the mass center and total mass of the entire tub-drum assembly without the three weight balancers;  $Z_{mcfu}$ ,  $Z_{mefd}$  and  $Z_{mcr}$  are, respectively, the mass center  $Z$  coordinates of the front-up, front-down, and rear weight balancers; and  $V_{fu}$ ,  $V_{fd}$ , and  $V_r$  are their respective volumes. The expression in Eq. (5) is also implemented in the Adams model, not as a design variable, but as a function expression to calculate  $\rho_r$  automatically, when the design variable  $DV\_MD$  for the mass density  $\rho_f$  is changed. The minimum value for  $DV\_MD$  is determined by a physical lower limit that ensures the rear weight balancer mass cannot be negative. Specifically, the minimum mass density of the front weight balancers is determined by setting that of the rear weight balancer to zero.

**Damper Coefficient, Front Damper Side Angle, and Rear Damper Side Angle**

The design variable  $DV\_visco\_C$  for the damping coefficient of the four simple dampers is added to the washing machine model with a nominal value of 0.5 (kgf.s/mm). As discussed, in total, there are four dampers in the washer model. To facilitate the presentation below, we denote the front right damper as “damper A”, the front left damper as “damper B”, the rear right damper as “damper C” and the rear left damper as “damper D”, as shown in Fig. 6a. In order to parameterize dampers’ side angle, i.e.,  $\gamma_1$  and  $\gamma_2$ , as shown in Fig. 4b, two DVs are added to vary the  $Z$  coordinate of the damper’s lower endpoints connected to the bottom frame:  $DV\_DFR$  (the  $Z$  coordinate of marker  $m$  and  $p$ , respectively, attached to damper A and B) and  $DV\_DRR$  (the  $Z$  coordinate of marker  $f$  and  $r$ , respectively, attached to damper C and D). Since dampers A and B, respectively, at the right and left, are perfectly symmetric to the  $Y$  axis, they share the same side damper angle ( $\gamma_1$ ). Therefore, only damper A’s side angle is parameterized and referred to as  $\gamma_1$ . Likewise, for the dampers at the back (dampers C and D), only damper C’s side angle is parameterized and denoted as  $\gamma_2$ . After parameterizing  $\gamma_1$  and  $\gamma_2$  at the right side, the damper B and D at the left will be updated automatically using proper functions in ADAM View, which allows the left dampers to follow their counterparts on the right side. The design

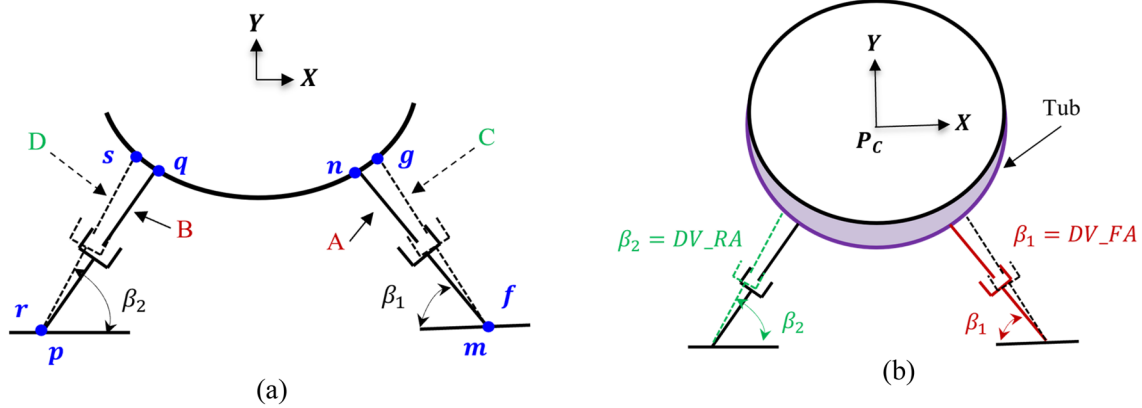


**Fig. 6** (a) the schematic drawings showing the upper and lower end points for all dampers and (b) The schematic drawings showing the front dampers' front angle ( $\beta_1$ ) and the rear dampers' front angle ( $\beta_2$ )

variable DV\_DFR alters the side angle of dampers A and B, while DV\_DRR changes the side angle of dampers C and D. The range of global Z coordinates of all lower endpoints for DV\_DRR and DV\_DFR must be consistent with the feasible range of the side angles  $\gamma_1$  and  $\gamma_2$  to ensure that the bottom markers  $m$ ,  $p$ ,  $f$  and  $r$  in Fig. 4b do not lie outside the physical domain of the bottom frame. In addition, the nominal value for both DV\_DFR and DV\_DRR is determined using the existing damper geometry data from the existing washing machine model.

Each damper consists of two body parts, a piston and a cylinder. Take Damper A as an example: it has marker  $m$  attached to the piston and marker  $n$  attached to the cylinder. Each marker defines a local coordinate system attached to the body. An orientation function below is utilized (one of the existing functions in the expression builder provided by Adams view) for the alignment of the line connecting the marker  $m$  and marker  $n$  to make sure that the damper's piston and cylinder are perfectly aligned in case either marker  $m$  or marker  $n$  is moved from its original place during design modifications.

**ORI\_ALONG\_AXIS** (markers  $m$ , markers  $n$ , the local Z axes).

This function returns the alignment of a specified axis from one coordinate system to another. In this case, the local Z axes of the markers  $m$  and  $n$  are aligned with the orientation function and always point toward each other when the location of the bottom marker is changed. The same procedure is employed for the alignment of the rest of the dampers.

### Front Damper Front Angle and Rear Damper Front Angle

Two design variables DV\_FA for the front angle of the front dampers and DV\_RA for the front angle of the rear dampers, i.e.,  $\beta_1$  and  $\beta_2$ , respectively, are added to the Model in Adams View for model parameterization and optimization as shown

in Fig. 6b. As discussed above, dampers B and D at the left are perfectly symmetrical, respectively, in relation to dampers A and C at the right; therefore, they share the same front damper angle. Consequently, only front angle of damper A is parameterized and referred to as  $\beta_1$ . Similarly, for the dampers at the back (dampers C and D), only the front angle of damper C is parameterized and denoted as  $\beta_2$ . The damper B and D at the left follow their counterparts at the right side accordingly. The nominal values for  $\beta_1$  and  $\beta_2$  are determined using the front and rear damper geometry data in the Adams washer model, respectively, using Eqs. (6) and (7):

$$\beta_1 = \tan^{-1} \left( \frac{Y_n - Y_m}{X_m - X_n} \right) \quad (6)$$

$$\beta_2 = \tan^{-1} \left( \frac{Y_g - Y_f}{X_f - X_g} \right) \quad (7)$$

where subscript  $n$ ,  $m$ ,  $g$ , and  $f$ , respectively, denote the upper and lower endpoints for dampers A and C as shown in Fig. 6a. The initial angle range from  $-5^\circ$  to  $+5^\circ$  is used for both  $\beta_1$  and  $\beta_2$ . However, two physical constraints affect the actually achievable range, corresponding to the two extreme cases when the damper becomes tangential to the cylindrical surface from the upper or lower side of the cylinder.

The angle  $\beta_1$  is parametrized by moving marker  $n$  on the cylindrical surface of the tub without the coupling between the damper side angle and front angle as shown in Fig. 6b. During design modifications, the marker  $n$  is restricted to moving along the elliptical curve formed by the plane passing through dampers A and B and intersecting the tub's cylindrical surface. Meeting these aforementioned conditions, the global coordinates of marker  $n$  can be



parameterized by  $\beta_1$  and the elliptical curve for the upper end points of damper A and B. In order to determine marker  $n$ 's coordinates, the following three equations are used.

In Eq. (8) below, the global X and Y coordinates of marker  $n$  are related to  $\beta_1$

$$X_n = X_m - (Y_n - Y_m) \cot \beta_1 \tag{8}$$

The second equation represents the parametric equation defining the plane that passes through the damper A and B in such a way that if the coordinates of each marker ( $m, n, p$  and  $q$ ) on dampers A and B are changed, the plane would move in space accordingly. Obviously, this plane, given by Eq. (9), is a function of the global coordinates of markers  $m, n, p$  and  $q$ . Note that the coordinates of marker  $m$  and  $p$  are already parameterized through the damper's side angle as discussed in Sect. "Damper Coefficient, front Damper Side Angle, and Rear Damper Side Angle" above.

$$\begin{aligned} & [(t_3(Y_n - Y_m) - t_2(Z_n - Z_m))(X_n - X_q)] \\ & + [(t_1(Z_n - Z_m) - t_3(X_n - X_m))(Y_n - Y_q)] \\ & + [(t_2(X_n - X_m) - t_1(Y_n - Y_m))(Z_n - Z_q)] = 0 \end{aligned} \tag{9}$$

where

$$t_1 = (Z_q - Z_p); t_2 = (Y_q - Y_p); t_3 = (Z_q - Z_p)$$

Due to symmetry, Eq. (9) will be simplified as follows:

$$t_3(Y_n - Y_q) - t_2(Z_n - Z_q) = 0 \tag{10}$$

The third equation to be determined is the cylindrical surface of the tub for marker  $n$  on damper A. As shown in Fig. 7, three coordinate systems are introduced: the global coordinate system ( $XYZ$ ), the local coordinate system before tilting ( $X'Y'Z'$ ), and the local coordinate system after

tilting ( $X''Y''Z''$ ). The origin of the global coordinate system is  $O(0, 0, 0)$ . The global coordinate system ( $XYZ$ ) shown in Fig. 7 is the same as the one introduced in the Adams View. Also recall that the tilt angle  $\theta$  of the axis of rotation, from the back of the tub to the front of the tub, is approximately  $5^\circ$  as presented earlier.

The global Y coordinate of the tub axis increases linearly from the rear end to the front end of the tub. According to the right-hand rule, the tub is rotated from the horizontal orientation (with its cylindrical axis along the  $Z'$  axis) to the tilted orientation (with its cylindrical axis along the  $Z_e$  axis) by  $-\theta$  about its local  $X'$  axis. The point  $P_c$  in Fig. 7 is the shaft mass center (introduced earlier) which is the origin of the local coordinate system before and after tilting of the shaft and the tub. Since the tub is rotated about its local  $X'$  axis during tilting, the axes  $X, X'$  and  $X_e$  are all parallel. The tilted cylindrical surface of the tub in the tilted coordinate system ( $X''Y''Z''$ ) has a simple form given by Eq. (11)

$$X''^2 + Y''^2 = R^2 \tag{11}$$

where  $R$  is the radius of the cylindrical surface for marker  $n$  on damper A, and its value is given by the distance from marker  $n$  to the tilted axis of rotation of the tub, i.e.,  $R = 349.8107$  mm. Assuming that  $E_e(X_e, Y_e, Z_e)$  is the coordinate vector of a point in the  $X''Y''Z''$  coordinate system and  $E(X, Y, Z)$  is that of a point in the  $XYZ$  coordinate system, the coordinate values of  $E_e$  and  $E$  in their respective coordinate systems are related through a transformation matrix  $T_{X_eTS}$  as following:

$$E'' = T_{X''TS} (E - P_c) \tag{12}$$

where  $P_c$  stands for the coordinate vector of point  $P_c$ , and

$$T_{X''TS} = \begin{bmatrix} 1 & 0 & 0 \\ 0 & \cos(\theta) & -\sin(\theta) \\ 0 & \sin(\theta) & \cos(\theta) \end{bmatrix}$$

Utilizing Eqs. (11) and (12), the equation of the cylindrical surface in the global coordinate system can be determined by

$$\begin{aligned} & [X_n - X_{P_c}]^2 + [(\cos(\theta)Y_n - \sin(\theta)Z_n) \\ & - (\cos(\theta)Y_{P_c} - \sin(\theta)Z_{P_c})]^2 = R^2 \end{aligned} \tag{13}$$

where  $X_n, Y_n$  and  $Z_n$ , again, represent marker  $n$ 's coordinates in the global coordinate system. Equation (13) also governs any cylindrical surface that shares the tilted axis of rotation with the tub. Thus,  $(X_n, Y_n, Z_n)$  as three unknowns can be obtained by solving Eqs. (8), (10) and (13), yielding

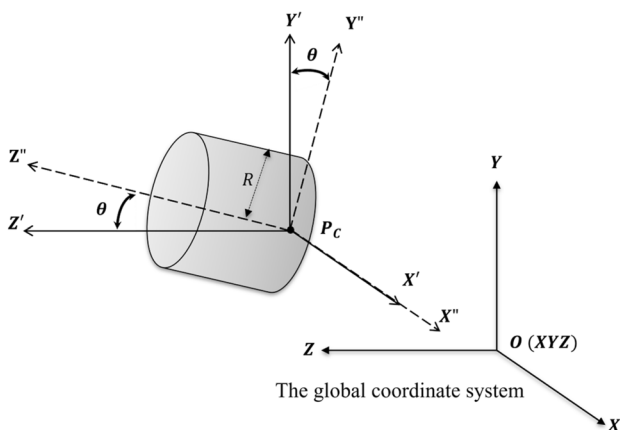


Fig. 7 The schematic showing the cylindrical surface of the tub in the global and local coordinate systems

$$\begin{aligned} Y_n &= \frac{-r - \sqrt{r^2 - 4qs}}{2q} \\ X_n &= q_1 - w_1 Y_n \\ Z_n &= w_3 Y_n + (-w_3 Y_m + Z_m) \end{aligned} \quad (14)$$

where,

$$\begin{aligned} q_1 &= X_m + Y_m \cot \beta_1 \\ w_1 &= \cot \beta_1; \quad w_2 = \frac{b_2 t_3}{t_2}; \quad w_3 = \frac{t_3}{t_2} \\ r_1 &= \cos \theta; \quad r_2 = \sin \theta \\ r_3 &= r_1 Y_0 - r_2 Z_0 \\ q &= w_1^2 + (r_1 - w_2)^2 \\ r &= 2((r_1 - w_2)(w_2 Y_m - r_2 Z_m - r_3) - q_1 w_1) \\ s &= (w_2 - r_2 Z_m - r_3)^2 + q_1^2 - R^2 \end{aligned} \quad (15)$$

The global coordinates  $X_n$ ,  $Y_n$  and  $Z_n$  presented in Eq. 14 are utilized to parameterize the front right damper's coordinates (i.e., marker  $n$ 's coordinates). These expressions are implemented in the Adams model by the expression builder as a function expression to automatically calculate marker  $n$  locations for the left and right dampers at the front (i.e., damper B and A) when design variable DV\_FA for  $\beta_1$  is changed. The same implementations are followed to parameterize design variable DV\_RA for the rear dampers' front angle ( $\beta_2$ ).

### Gaussian Process Model

As a widely used probabilistic surrogate model, Gaussian Process (GP) approximates objective functions by modeling a distribution of random variables to fit a set of data points [22]. This feature makes them well-suited for approximating true objective functions in BO.

Given the total number  $n$  observations or sample points over the finite domain  $\mathcal{D}_n = (x, y)$ , which are used as the training data set, where  $X = [x_1, x_2, \dots, x_n]$  is the input with  $n$  as the number of sample points, and  $Y = [y_1, y_2, \dots, y_n]$  is the corresponding response or output. The (GP) model operates under the premise that the observed data adhere to a Gaussian distribution. The objective therein is to formulate a regression framework aimed at predicting output response denoted as  $y$ , for a new data point  $x$  [22]. GP regression uses a multivariate normal prior distribution, where the regression is specified through two functions: a mean function that is a vector and a covariance or kernel function which is a matrix [24]. The kernel is deliberately selected in such a way that data points  $x_i$  and  $x_j$ , which lie in close proximity in the input space, exhibit a strong positive correlation. This reflects the underlying notion that these points should

possess function values that are more alike compared to points situated at a distance from each other [24].

One of the most common kernel functions for GP are Matern class kernels, which are discussed in detail in [25]. In this study, Adaptive Relevance Determination (ARD) Matern 5/2 is used, which enables the GP model to learn the key observed features [26]. MATLAB's build-in function, *fitrgp*, is used for the Gaussian Process modeling in this study. The *fitrgp* function allows specifying the kernel function through *KernelFunction*. This functionality allows users to designate a predefined function as the kernel in GP modeling. The ARD Matern 5/2 kernel was selected in this study.

### Adaptive Sampling

Prior to modeling the objective functions and its dependence on various design variables, it is critical to establish the initial set of data points (initial sampling) with a consistent level of model accuracy across the multi-dimensional design space. The significance of the initial sampling lies in the high cost associated with the computation of generating each individual data point, which makes the selection of a highly informative set of initial samples challenging [27].

The statistical sampling plan called Latin Hypercube Sampling (LHS) is chosen to randomly select initial sample points to fill the entire design space. LHS is selected since it is one of the most widely used methods to generate random sampling points to initiate optimization algorithms, which guarantees an even distribution of samples within the range of design variables and salient representation of all regions within the design space [28, 29]. More specifically, the LHS of a size  $N$  is generated by segmenting the distribution of each input design variable into  $N$  equal probability proportions, and sampling exactly one value from each division [29]. This segmentation (also called stratification) allows LHS to have a wider and more efficient coverage on the entire DVs domain [30]. The MATLAB function, *lhsdesign*, is utilized to obtain  $N$  sample points considering the DVs lower and upper bound, and  $N$  is a user input.

After constructing a full set of initial space-filling samples, the algorithm utilizes the response surface obtained from the GP and iteratively updates the model with additional information through an approach called adaptive sampling. Although the ideal scenario is to train the model with complete information, it is infeasible in reality as the computational resource is limited [31]. Adaptive sampling strategically selects certain data point based on the acquired knowledge from the GP model specifically in the targeted area [31, 32]. The newly selected infill point dynamically adds a data to the existing training data set and related information to the model, which

intelligently and progressively improves the quality of the optimization [33].

The selection of the infill criterion plays a crucial role in the optimization performance, which is normally achieved by maximizing the acquisition functions. In this paper, two different acquisition functions, proven effective in our prior effort [32] are utilized to perform BO: statistical lower bound (LB) and expected improvement (EI). The LB is an approach to balance exploitation and exploration with the formula below [34]:

$$LB(x) = \hat{y}(x) - A\hat{s}(x) \quad (16)$$

where  $\hat{y}(x)$  and  $\hat{s}(x)$  are respectively, prediction and the square root of predicted variance. As the value of  $A$  goes closer to zero, the effect of  $\hat{y}(x)$  will be more important, emphasizing exploitation (pure exploitation), while as  $A$  gets closer to  $\infty$ ,  $LB(x)$  aligns more with exploration (pure exploration). In other words,  $A$  is a constant that controls the balance between exploitation and exploration, which is set to be 2 in this paper following our prior work [32]. The other acquisition function used in this paper is the expected improvement (EI), which is defined in Eq. 17 below

$$E[I(x)] = \begin{cases} (y_{min} - \hat{y}(x))\Phi\left(\frac{y_{min} - \hat{y}(x)}{\hat{s}(x)}\right) + \hat{s}(x)\varphi\left(\frac{y_{min} - \hat{y}(x)}{\hat{s}(x)}\right) & \text{if } s > 0 \\ 0 & \text{if } s = 0 \end{cases} \quad (17)$$

where  $\Phi(x)$  represents the cumulative distribution function and  $\varphi(x)$  is the probability density function [34]. In the infill methods,  $y_{min}$  is the best observed value that in our case would be the minimum observed sampling, and  $E[I(x)]$  represents the area enclosed by the Gaussian distribution below the minimum of the optimization model found at the current iteration.

## Genetic Algorithm

The next step is to determine the infill location for adding new data in each iteration of optimization, which essentially requires an efficient search algorithm to find the global optimal value of the acquisition function above.

Genetic Algorithm (GA), one of the most popular stochastic optimization algorithms [35] is chosen as the infill search tool. GA is an evolutionary algorithm inspired by Darwin's theory nature's fittest [36] which simply means the fittest gene survive to the next generation. Like other standard evolutionary algorithms (EAs), GA uses three fundamental operators for sequential reproduction: selection, crossover, and mutation [35]. In the selection operator, individuals with superior fitness scores are favored, and thus, more likely to propagate their genetic information into the next generation of solutions [37]. Using both selection and crossover operators, GA generates new offsprings with better potential to reach optimum solution. The mutation operator

inserts random genetic modifications into the offspring solutions, preserving population diversity, and avoiding over-divergence from the optimum solution [37].

Using the aforementioned steps, this technique employs guided randomized exploration intelligently, supplemented by the integration of historical data. This approach systematically advances the search process within areas of potential solutions identified by previous findings, resulting in enhanced performance [37]. This adaptive feature makes GA a strong and robust tool to solve complex problems with multiple parameters in a large space for a satisfactory answer with lower computational cost in optimization algorithms [38]. Due to the reliability, adaptability and its convergence rate, GA is suited to this task, and it is used as the search algorithm in BO. In this paper, MATLAB's built-in function, *ga*, is used to search for the global optimum value of the acquisition function in the algorithm. This function optimizes the objective function based on user-input parameters and variables, including the total number of DVs and the lower and upper bounds of each design variable. Our modeling approach demonstrates great robustness, with MATLAB's default GA configurations. Some of the configuration variables are briefly discussed here for clarity.

The number of candidate solutions evaluated in each generation by the GA is called population size, which depends on the number of variable ( $NV$ ). Typical population size is 50 or 200; 50 for a smaller number of variables specifically for  $NV \leq 5$ , while a larger number of variables or  $NV > 5$  uses a population size of 200. Two models are investigated in this paper, which will be elaborated on in Sect. "Result and Discussion": one model comprises 5 DVs, while the other model encompasses 9 DVs. In the case study of the former, the population size will be set to 50, whereas for the scenario with 9 DVs, the population size is increased to 200. The mutation function utilized to generate mutation children in the 'ga' function is 'mutationgaussian'. This default mutation function adds a random number sampled from a Gaussian distribution with a mean of 0 to each element of the parent vector. The default selection function in the 'ga' function is 'selectionstochunif'. This function organizes a line where each parent corresponds to a segment of the line, the length of which is proportional to its scaled value. As the algorithm progresses along the line, it takes steps of a uniform size. At each step, the algorithm assigns a parent from the segment it reaches, with the initial step beginning with a uniformly distributed random number smaller than the step size. The population fraction created by the crossover function at the next generation in the *ga* algorithm is chosen to be 0.8. The *ga* function default tolerance is 1.0E-06. Additionally, the maximum number of iterations permitted before the termination of the GA in MATLAB is denoted by  $NV \times 100$ . However, the termination criterion is determined

by the user-defined maximum number of iterations. Once this criterion is met, the algorithm terminates.

## Result and Discussion

In this section, we will perform a parametric analysis using the model with nine design variables (DVs) followed by optimization result and discussion. The parametric analysis conducted in this paper includes changing each individual design variable from its lower bound value to the upper bound value to evaluate how the maximum X displacement amplitudes at the front sensor changes with the design variable. For optimization, two case studies, respectively, involving five and nine DVs are conducted and analyzed, and the effect of the acquisition functions on BO convergence is also investigated.

## Parametric Analysis

The analysis starts with a single simulation, in which all DVs are set to their standard values. The simulation model with all DVs set to their standard values is called the standard configuration. The details of the solver settings are presented in our previous work [20]. Figure 8a–c portray the time-varying response for the displacement amplitude along X, Y and Z direction at the front sensor for the standard configuration. Each data series consists of two parts, a transient state and a quasi-steady state. It is clear from Fig. 8a–c that the maximum displacement in all three directions always occurs in the transient stage.

Subsequently, the parametric analysis is performed to investigate the impacts of individual DVs only on the maximum X displacement amplitudes. To facilitate visualization and interpretation of the results, each DV's range is normalized between 0 and 1. Each curve in Fig. 9 then depicts the variation of the Front sensor maximum displacement amplitude along X direction when one of the DV is set to

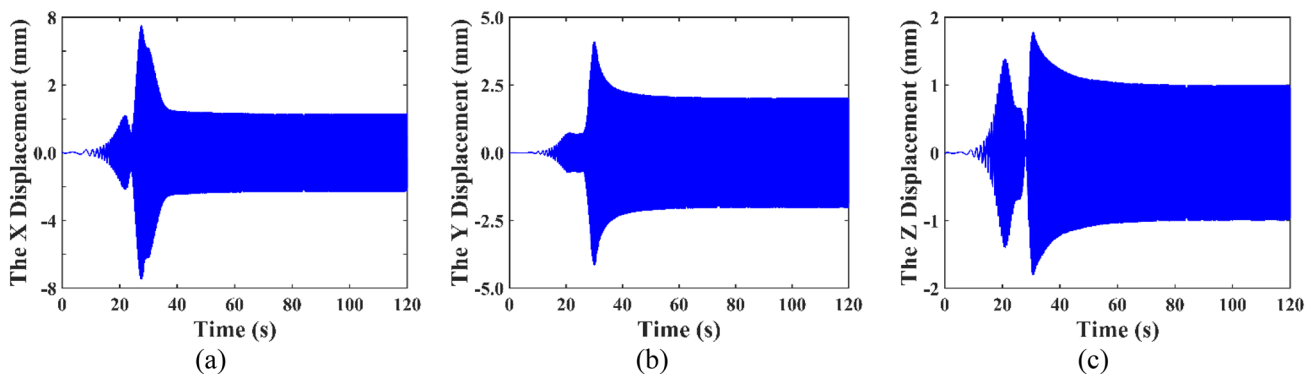
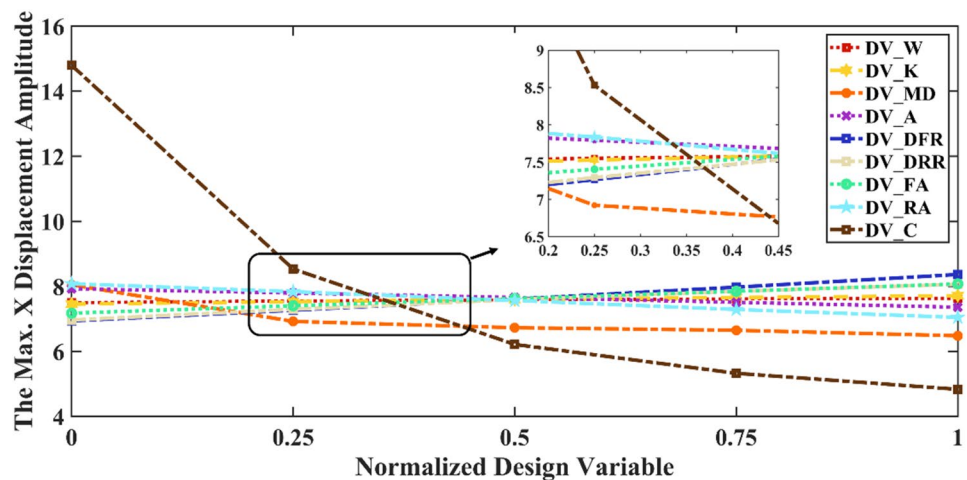


**Fig. 8** The simulation results for the standard configuration: (a) the front sensor X displacement; (b) the front sensor Y displacement; and (c) the front sensor Z displacement

**Fig. 9** The parametric analysis considering all nine DVs for the variation of the front sensor maximum X displacement amplitude





a different value in the normalized range, viz., 0, 0.25, 0.5, 0.75, and 1, and the rest of DVs remain unchanged (i.e., keeping their standard value). The maximum X displacement amplitude is positively proportional to five DVs out of nine, including the rotation speed ( $w$ ), spring stiffness ( $K$ ), front damper Z Coordinate (DV\_DFR), rear damper Z Coordinate (DV\_DRR), and front damper front angle ( $\beta_1$ ). That is, when these five DV values increase, the maximum X displacement also grows. On the other hand, the maximum X displacement amplitude increases when the rest of the DVs decrease their values, viz., the spring angle ( $\alpha$ ), rear damper front angle ( $\beta_2$ ), mass density ( $m$ ), and damping coefficient ( $C$ ).

The impacts of individual DVs on the maximum displacement amplitudes along Y and Z is discussed in detail in the previous study [20]. The parametric analysis confirms that the magnitude of the maximum displacement amplitude is dependent on all the 9 DVs. As discussed in Sect. “[Problem Description](#)”, the goal of the study is to minimize the maximum displacement amplitude of the tub to avoid any potential collision. The above analysis clearly suggests that there is a complex nonlinear relationship between the maximum amplitude in each direction and the nine DVs. Thus, it is a formidable challenge to identify the optimal design manually or in a straightforward manner. Instead, the BO algorithm with adaptive sampling is utilized to facilitate and automate the design of this front-load washing machine. To evaluate BO-based optimization, two different case studies, respectively, involving 5 DVs and 9 DVs with an increasing level of complexities are considered, followed by comparison between them, results, and discussion.

### Case Study 1: Optimizing Model with 5 DVs

The case study in this section uses a washing machine model with a total number of five DVs, including rotation speed, spring stiffness, spring angle, mass density, and damper coefficient. The BO starts with 20 training data obtained through the LHS hypercube sampling. The two different acquisition functions for adaptive sampling are employed

and compared in the BO. The first algorithm uses the lower bound (LB) type of acquisition function and the second one utilizes the expected improvement (EI) as presented above. Table 2 presents the result of the optimization including the optimal DV values. Again, each simulation starts with 20 initial training data sets and continues with 50 additional samples determined by adaptive sampling.

As shown in Table 2, the maximum amplitude of the front sensor X displacement obtained by BO with the LB acquisition function is 3.4505 mm, and the optimum design is obtained at iteration No. 43. Similarly, when BO with the EI acquisition function is employed, the amplitude of the front sensor X displacement reaches the minimum value of 3.4506 mm with almost the same DV values for the optimal parameter set presented in Table 2, although the optimum design is attained much faster and at iteration No. 19. It is also interesting to observe that BO with the LB acquisition function can reach 2.4506 (the optimum design found by EI) at iteration No. 36, which, however, is still slower compared to EI.

The evolving optimization results during iterations for the washing machine model parameterized with 5 DVs utilizing the LB and EI acquisition functions are presented in Fig. 10. According to Fig. 10a, the maximum amplitude of the front sensor X displacement found by BO with LB suddenly drops because the initial design represents the maximum amplitude for the standard configuration. Following a decay from the initial design, it gradually decreases until it does not change after iteration No. 43. Figure 10b illustrates the maximum amplitude of the front sensor X displacement found by BO with EI. A rapid decay at the beginning of the plot is observed again, which shows the difference between the optimal value found by the optimizer and the maximum amplitude obtained from the standard configuration. The optimal value is found at the iteration of No. 19, and after that the maximum amplitude remains as a constant till the end of the optimization. Considering the fact that the optimization with both acquisition functions and infill techniques lead to almost the same DV set except for the rotation speed and maximum amplitude, and the BO with EI method

**Table 2** Five design variables utilized in case study 1 with the optimum DV values obtained using the LB and EI acquisition functions

Optimal Parameter Set			
Symbols	Definitions	LB	EI
W	Rotation speed (rpm)	809.9439	800.0000
K	Spring Stiffness (kgf/mm)	0.6500	0.6500
$\alpha$	Spring angle ( $^\circ$ )	5.0000	5.0000
MD	Mass density (kg/mm <sup>3</sup> )	9.3749E-06	9.3749E-06
C	Damper coefficient (kgf.s/mm)	1.5000	1.5000
F_X	Maximum displacement (mm)	3.4505	3.4506
IN	The optimum design's iteration number	43	19



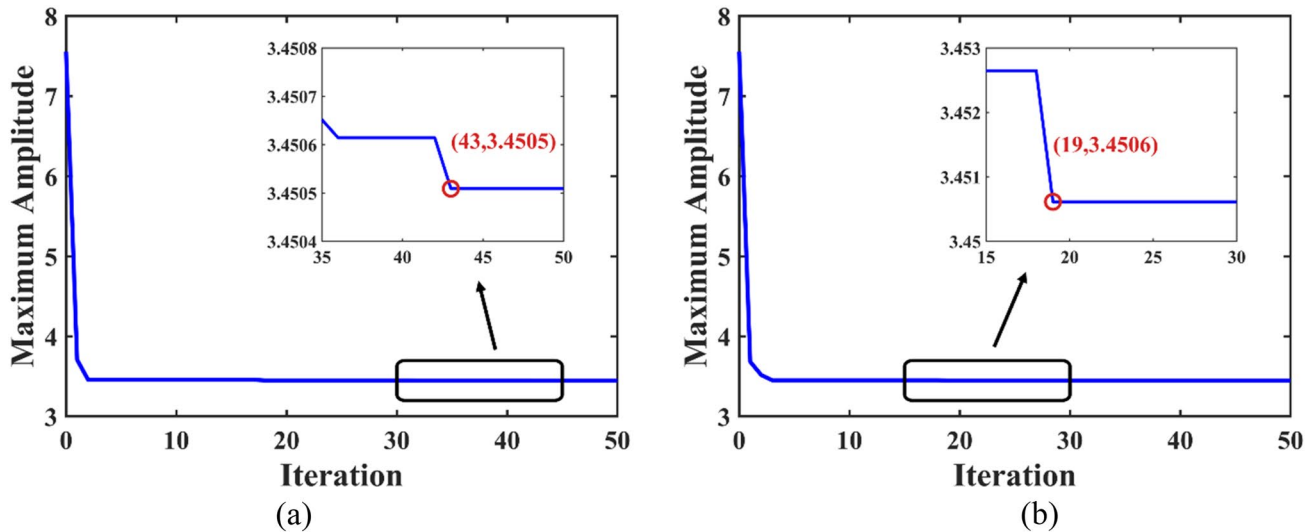


**Fig. 10** Convergence of the maximum displacement for the washer model parameterized with 5 DVs using different acquisition functions: (a) LB and (b) EI

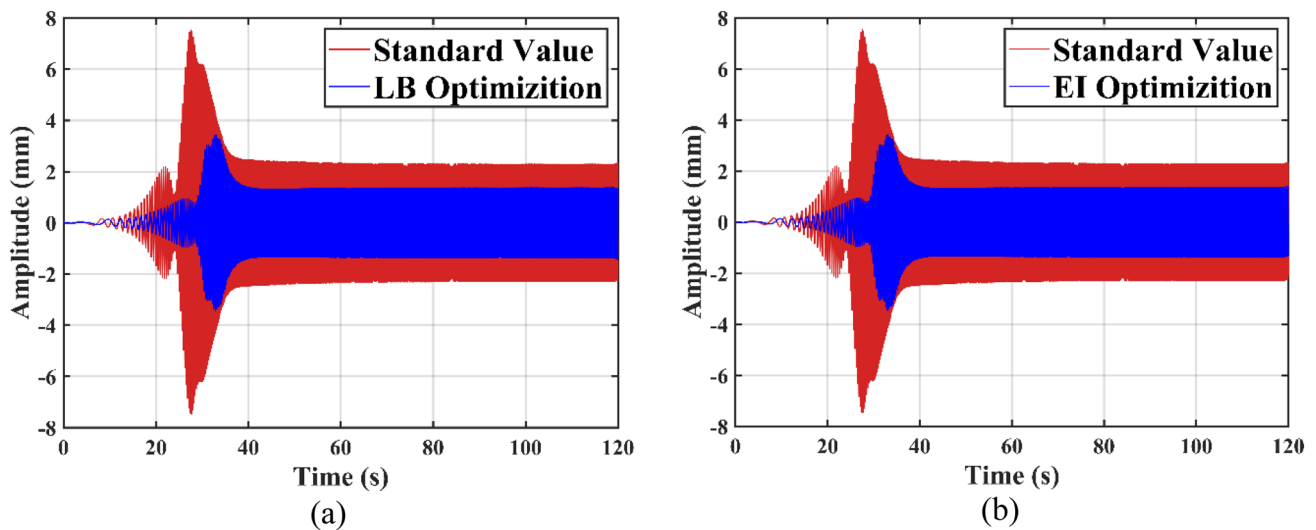


**Fig. 11** Comparison of results of the maximum amplitude for the standard configuration and the optimal DV values for case study 1: (a) using LB and (b) using EI as the acquisition function

can reach the optimal design faster than the BO with LB, it is safe to deem that the former is more computationally efficient.

As mentioned earlier, the simulation model with all design DVs set to their standard values is called the standard configuration. Figure 11 compares the time series of the X displacement amplitude at the front sensor X in two simulations: one takes all standard values of all DVs (the red curve) and the other sets all DVs to the optimal values found by the optimization algorithm (the blue curve). Figure 11a illustrates the temporal response for BO with LB, and obviously the maximum displacement amplitude for the

optimum design stays much lower throughout the time span compared to that obtained with the standard configuration. The purpose of optimization is to find an optimum set of DV values with the lowest possible (minimal) value of the maximum displacement amplitude relative to the washing machine frame during operation in order to reduce unfavorable movement of the machine and improve its safety, which is confirmed by the present BO results. Also, Fig. 11b illustrates the temporal response for the design obtained by BO with EI and the similar observation in displacement minimization is obtained.

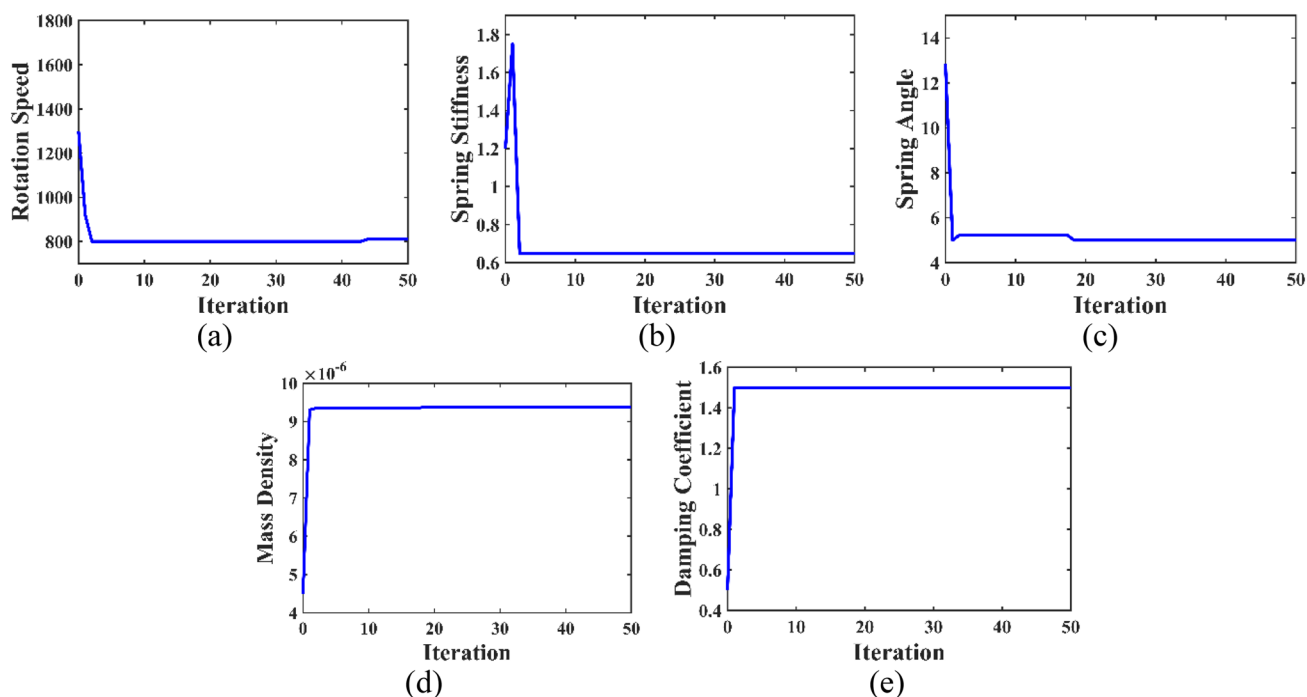


**Fig. 12** The variation of individual design variables with iteration throughout the optimization process for case study 1 with LB: (a) Rotation Speed, (b) Spring Stiffness, (c) Spring angle, (d) Mass Density, (e) Damper Coefficient

Figure 12a–e depicts the variation of each individual DV with iteration throughout the optimization process for Case Study 1 with LB. This case study comprises 50 iterations. At iteration 0, the vertical axis represents the standard value of the DV as provided in the software Adams View. In all figures, there is an abrupt change from the standard value to the optimal value of DVs found in BO at iteration 43, corresponding to the best minimum of the objective function (3.4505 mm) given in Table 2.

The optimal value for rotation speed in Fig. 12a happens at 809.9439 rpm (as given in Table 2) which is close to the lower bound after experiencing some variation with BO process. In both Fig. 12b, c, variations of the DVs of spring stiffness and spring angle with iteration are shown, with the optimal value approaching the lower bound assigned to the DV. Figure 12d displays the variation of mass density throughout the optimization process, showing a trend towards the upper bound. This finding supports the conclusion drawn in a previous study [20] that increasing mass density leads to a decrease in amplitude. Figure 12e demonstrates that the optimal value is reached at the maximum allowable value for the damping coefficient. This indicates that the highest value of the damping coefficient results in the lowest maximum amplitude in the front sensor X displacement. This observation further supports our previous finding [20] that greater damping coefficients are associated

with notably decreased amplitudes for the system under consideration.

Figure 13a–e depicts the variation of each individual DV with iteration throughout the optimization process for Case Study 1 with EI. All DVs have their optimum solution at iteration 19 as shown in Table 2. The optimum rotation speed in Fig. 13a aligns with the lower bound with some changes at the first couple of iterations. Both Fig. 13b, c show the variations of DVs spring stiffness and spring angle with iteration, consistently trending towards the lower bound. Figure 13d indicates the optimal mass density is found around the upper bound, resonating results from [20] that higher mass density correlates with reduced amplitude. In Fig. 13e, the optimal value coincides with the maximum allowed damping coefficient, reinforcing our prior discovery [20] that higher damping coefficients result in decreased amplitudes.

### Case Study 2: Optimizing Model with 9 DVs

In the next step, we extend our study to the model with 9 DVs and investigate the effect of the new DVs on the system. It should be noted that in the first case study, the only DV related to the dampers is the damping coefficient, while in this case study, four additional DVs are introduced to the washing machine model, which are the front/rear dampers side angle ( $\gamma_1$  and  $\gamma_2$ ) and the front/rear dampers front angle ( $\beta_1$  and  $\beta_2$ ). The model will be a function of the geometrical

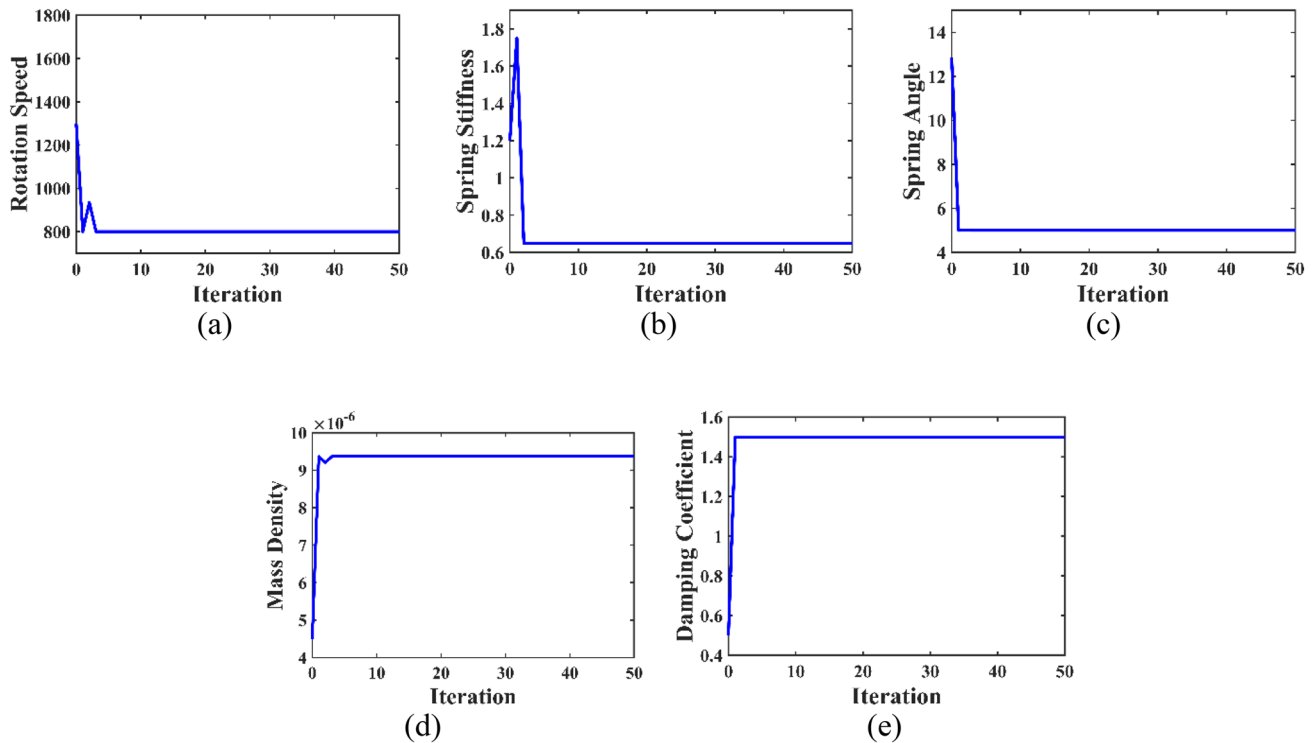


**Fig. 13** The variation of individual design variables with iteration throughout the optimization process for case study 1 with EI: (a) Rotation Speed, (b) Spring Stiffness, (c) Spring angle, (d) Mass Density, (e) Damper Coefficient

**Table 3** Nine design variables utilized in case study 2 with the optimum DV values obtained using the LB and EI acquisition functions

Optimal parameter set			
Symbols	Definitions	LB	EI
W	Rotation Speed (rpm)	822.4339	800.0000
K	Spring Stiffness (kgf/mm)	0.6500	0.6500
$\alpha$	Spring angle ( $^{\circ}$ )	16.5614	11.3126
MD	Mass Density ( $\text{kg}/\text{mm}^3$ )	9.3367e-06	9.3355e-06
C	Damper Coefficient (kgf.s/mm)	1.5000	1.5000
DFR	Front damper Z Coordinate (mm)	538.6186	537.9556
DRR	Rear damper Z Coordinate (mm)	147.4810	100.2430
FA	Front damper front angle ( $^{\circ}$ )	65.5000	65.5000
RA	Rear damper front angle ( $^{\circ}$ )	84.4000	83.5445
F_X	Maximum Displacement (mm)	2.5901	2.5468
IN	The optimum design's iteration number	46	26

position of dampers as well, and accordingly, the new DVs increase system complexity. In other words, the displacement amplitude observed by the sensor will be altered as the damper's geometry changes in design. It would allow for even more room for displacement minimization and design improvement.

In this study, the BO starts with 50 initial training data, which increases from 20 in the first case study to accommodate the higher dimension of the design space, i.e., the

number of DVs changes from 5 to 9. A total of 70 iterations (i.e., infills) in addition to the initial 50 data are used. Again, both acquisition functions: LB and EI are used, and their results are compared. Table 3 presents the result of the optimization including the optimal DV values. The optimal solution for the maximum amplitude of the front sensor displacement along the X-direction using the BO with the LB acquisition function is 2.5901 mm and found at iteration No. 46. On the other hand, the BO with the EI acquisition

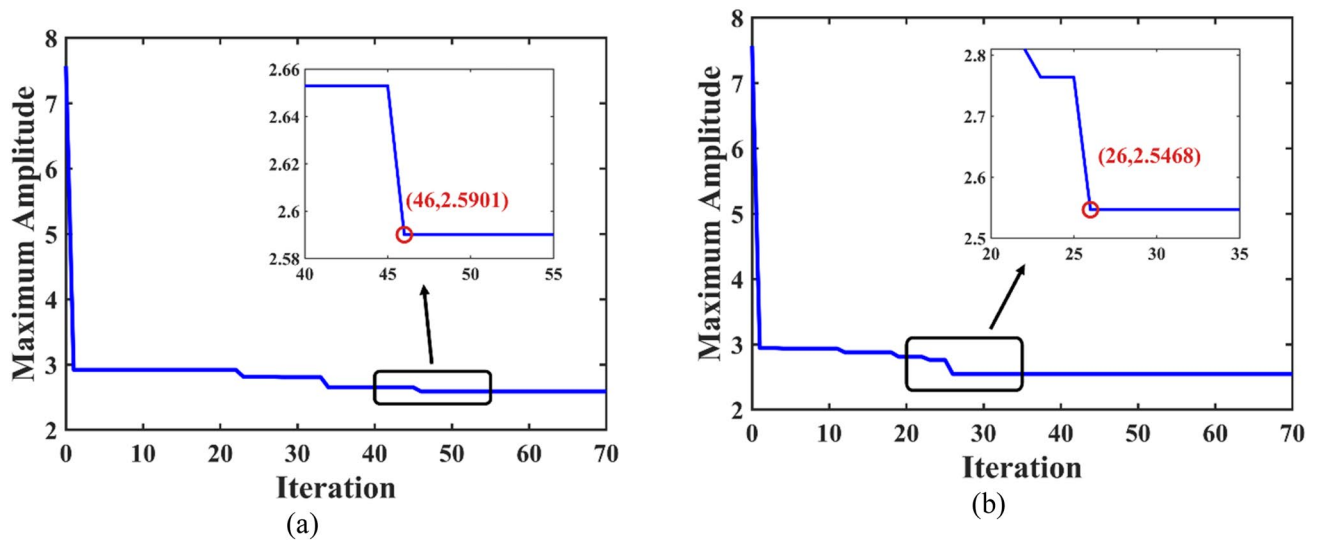


**Fig. 14** Convergence of the maximum displacement for the washer model parameterized with 9 DVs using different infill strategies: (a) LB and (b) EI

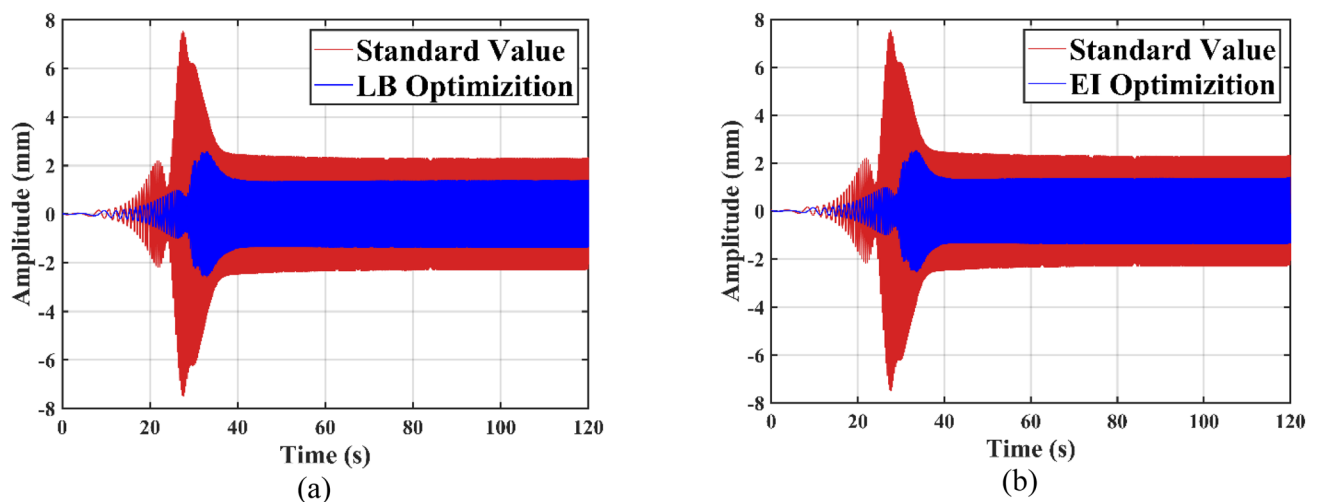


**Fig. 15** Comparison of results of the maximum amplitude for the standard configuration and the optimal DV values for the case study 2: (a) optimization using LB infill strategy and (b) optimization using EI infill strategy

function identifies an even better optimum solution with the amplitude of 2.5468 mm at iteration No. 26. These observations indicate that the BO with EI not only achieves a lower X displacement, but also accelerates the design optimization process dramatically.

The convergence of the optimization process for the washing machine model parameterized with 9 DVs is presented in Fig. 14. It shows that the amplitude of the X displacement initially decays rapidly, and then becomes saturated when it approaches the optimum. Although the profiles appear similar for both LB and EI acquisition functions, their convergence is quite different. Figure 14a shows

that the maximum displacement value for the BO with LB does not change after iteration No. 46. Additionally, Fig. 14b illustrates the maximum amplitude of the X displacement obtained with EI. It can be seen that the solution reaches the plateau at the 26th iteration. Since the BO with EI finds the optimum design with a lower number of infills, we can conclude that this infill strategy converges faster for the washing machine system with 9 DVs under consideration.

Likewise, the temporal responses for the second case study obtained by the BO with the LB and EI acquisition functions (in blue) are depicted in Fig. 15. Their results are also compared with those generated by the standard DV

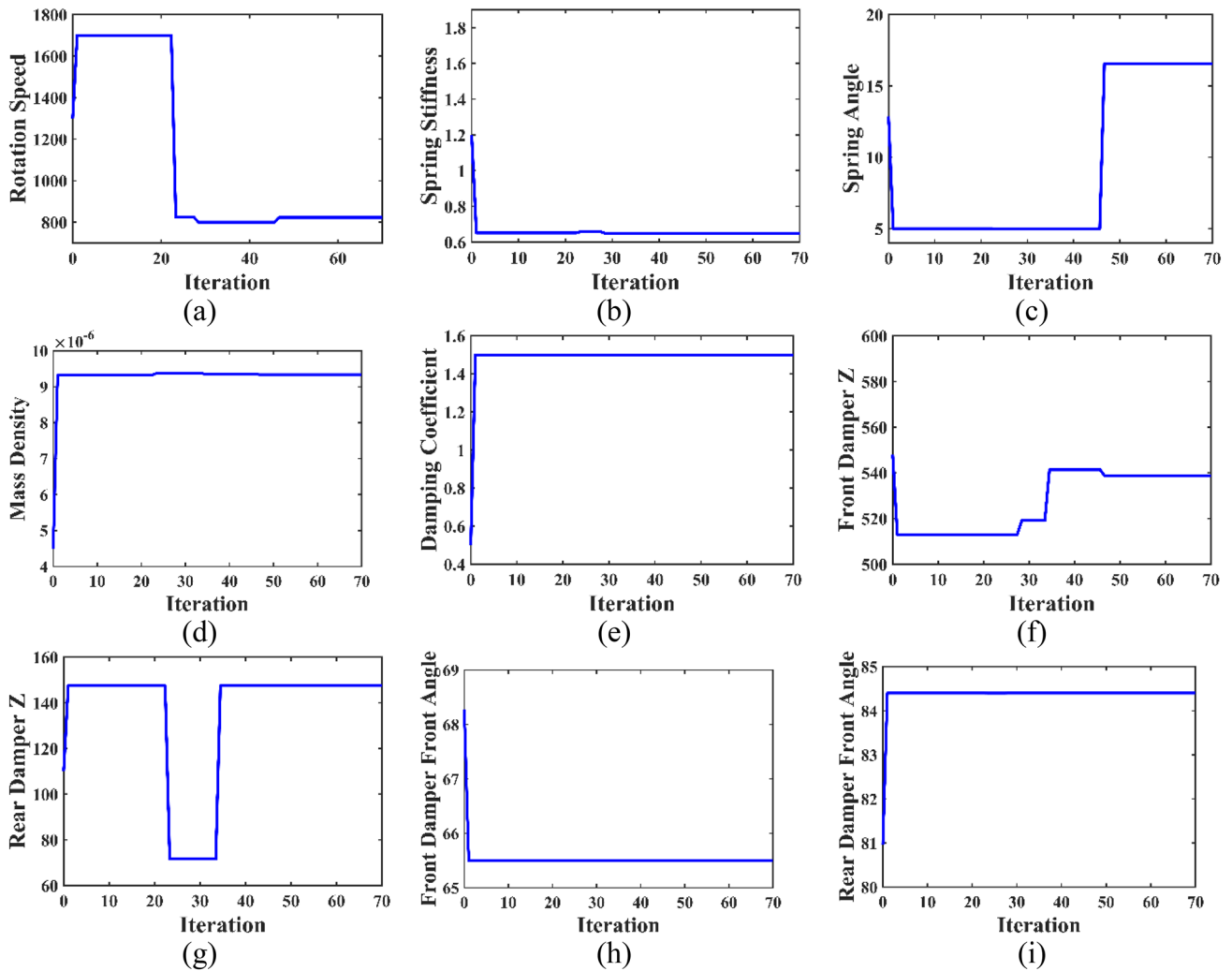


**Fig. 16** The variation of individual design variables with iteration throughout the optimization process for case study 2 with LB: (a) Rotation Speed, (b) Spring Stiffness, (c) Spring angle, (d) Mass Den-

sity, (e) Damper Coefficient, (f) Front damper Z Coordinate, (g) Rear damper Z Coordinate, (h) Front damper front angle, (i) Rear damper front angle

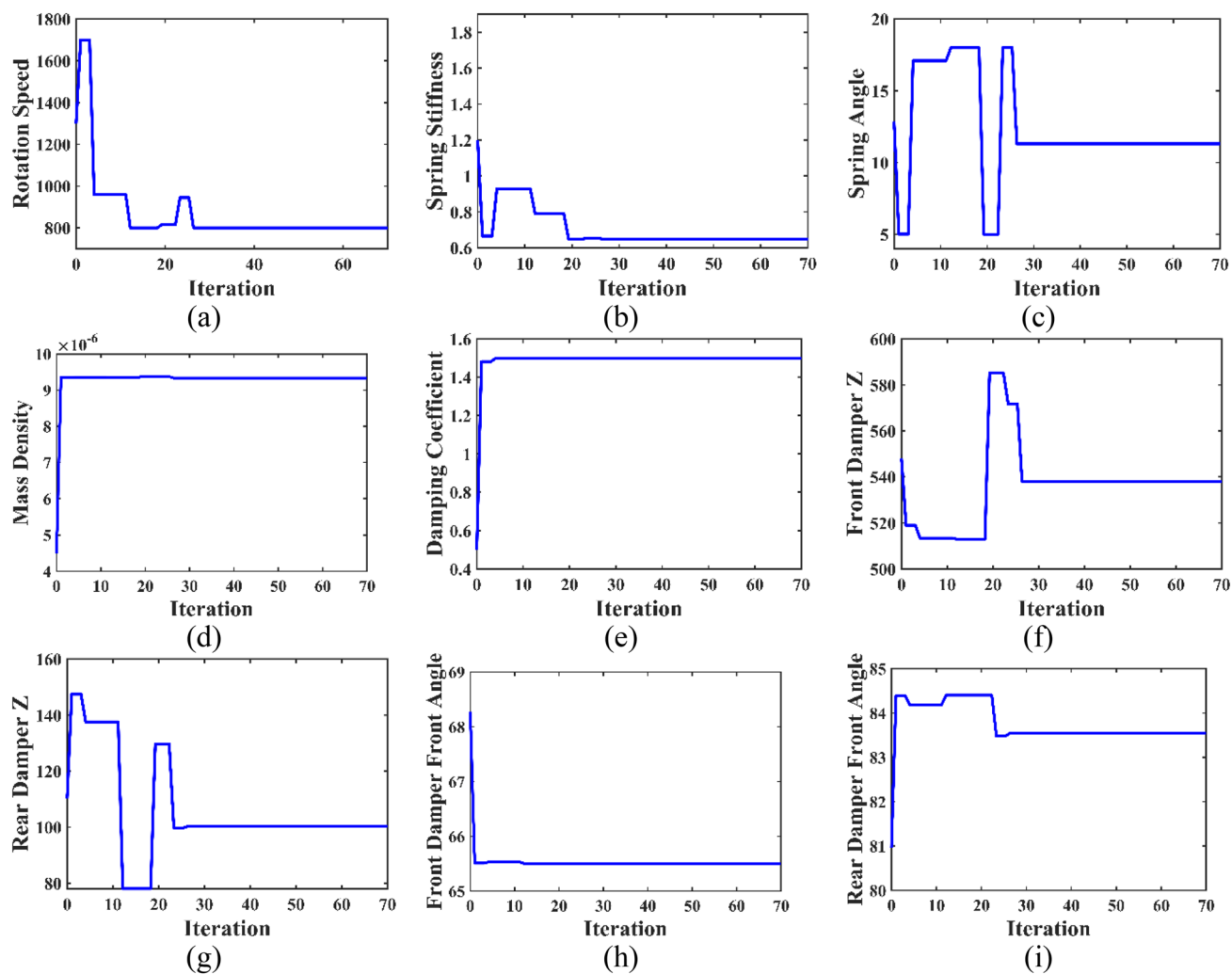
values (in red). Results in both Fig. 15a, b clearly exhibit that the displacement for the optimum design during the entire time span is dramatically lower compared to that with standard configuration and that with 5 optimal DV values above as well.

Figure 16a–i illustrate the variation of each individual DV with iteration during the BO process for Case Study 2 with LB. This case study spans a total of 70 iterations, with the vertical axis at iteration 0 representing the standard value of the DV. It can be observed in all Fig. 16a–i that DVs' optimal values occur at iteration number 46 (given in Table 3), and the DV value in each plot remains the same after this iteration.

Figure 16a illustrates the variation of the DV with iteration for the rotation speed. It can be observed that the DV eventually reaches its optimum at 822.4339 rpm

which is close to its lowest possible value after experiencing significant fluctuations, a trend not observed in the first case study. It is observed that the value of this DV changes during optimization until it reaches the optimal value at iteration 46 as shown in Table 3. The DVs variation for the spring stiffness and spring angle values with iteration in the BO process are depicted in both Fig. 16b, c, respectively. In both cases, fluctuations are observed throughout the optimization process. The optimum of spring stiffness occurs at the specified lower bound, while more variation is observed for spring angle during optimization. The optimal value for the spring angle is found at 16.5614 degree, which is between the bounds as shown in Fig. 16c. This particular variation of spring angle was not observed in the case study with 5 DVs. Figure 16d displays the variation of mass density throughout the optimization





**Fig. 17** The variation of individual design variables with iteration throughout the optimization process for the case study 2 with EI: (a) Rotation Speed, (b) Spring Stiffness, (c) Spring angle, (d) Mass Den-

sity, (e) Damper Coefficient, (f) Front damper Z Coordinate, (g) Rear damper Z Coordinate, (h) Front damper front angle, (i) Rear damper front angle

process, trending towards the upper bound, and Fig. 16e demonstrates that the optimal value occurs at the maximum value for the damping coefficient. These two later observations further support our previous finding [20] that greater damping coefficients are associated with notably decreased amplitudes, and higher mass density is associated with lower amplitude.

The variations of the front and rear dampers' Z coordinates, representing the side angles of the front and rear dampers, are shown in Fig. 16f, g, respectively. The front damper Z coordinate achieves its optimal value after some fluctuations during the BO process somewhere between the DV range at 538.6186 mm. The rear damper Z coordinate reaches its optimal value after multiple variations in the BO process and at iteration 46. It is observed that these two DVs exhibit noticeable variation throughout the BO process. The variation of the front damper front angles is given in

Fig. 16h, with the optimal value for this DV occurring at the lower bound. The last plot, Fig. 16i, shows the variation of the rear damper front angles, with the optimal value for this DV occurring at the upper bound.

Figure 17a–i show each individual DV change with iteration during the optimization for Case Study 2 with EI. In all plots it is observed that the optimum solution for DV happens at iteration 26 as shown in Table 3. Figure 17a depicts the variation of the rotation speed DV during the optimization process. It can be observed that, after significant fluctuations, the DV eventually converges to its optimal value at the lower bound. Figure 17b, c illustrate the changes in the spring stiffness and spring angle DVs, respectively, throughout the BO process. In both cases, DVs' values exhibit fluctuations along the optimization trajectory. The spring stiffness achieves its optimum value at its lowest value; however, the spring angle optimal value happens somewhere within

the range at 11.3126 degree at iteration 26 (see Table 3), which is where optimal solution for the maximum amplitude of the front sensor X displacement is found. Figure 17d shows the variation of the mass density DV, which trends towards the upper bound, and Fig. 17e demonstrates that the optimal value for the damping coefficient also occurs at its upper bound.

Figure 17f, g present the variations of the front and rear dampers' Z coordinates, respectively, representing the front and rear dampers' side angles. Both DVs reach their optimal values after multiple variations during the BO process, exhibiting substantial fluctuations. The optimum value of the front damper Z coordinate occurs at 537.9556 mm in the DV range at iteration 26. Based on Fig. 17g, the rear damper Z coordinate's optimal value happens at 100.2430 mm (see Table 3) in the DV range after some changes during BO process. It was observed that the optimal value for both front and rear dampers' Z coordinates happen within the range of the DV, which shows the importance of these parameters on the optimum solution found by BO. Figure 17h illustrates the variation of the front damper front angle DV, with the optimal value occurring at the lower bound. Finally, Fig. 17i depicts the variation of the rear damper front angle DV, where the optimal value is found somewhere between the bounds at 83.5445 degree (as presented in Table 3).

Studying both cases yielded some findings that can be summarized as follows:

The optimal values of the rotation speed and spring stiffness are consistently close to or at the lower bounds. The optimal values of mass density and damping coefficient occurred at the upper bounds of both DVs, supporting our key findings from the previous research study [20] that greater damping coefficients are associated with notably decreased amplitudes, and higher mass density is associated with lower amplitude.

The spring angle exhibited different optimal values for the model with 5 DVs or 9 DVs. In the case study with 9 DVs, the spring angle showed different behavior, and fluctuations of the DV value were observed throughout the BO process. The front and rear dampers' Z coordinates experienced significant fluctuations before reaching optimal values. In the case study with 9 DVs and the EI criterion, the fluctuations of the dampers' angles were more pronounced compared to the case study with 9 DVs with LB, potentially caused by more broad exploration of the parameter space. The rear damper front angle in Case study 2 with EI showed fluctuations and the optimum value happened within the range of the DV. These observations mentioned above prove that the dampers' side and front angles are important parameters affecting the washer model with 9 DVs to have a lower maximum displacement when compared to a model with a lower number of DVs.

## Conclusion

This paper presents parameterized dynamic modeling of a front-loading washing machine, which establishes the mathematical relationship between the vibrational characteristic and a thorough list of nine design variables. The main purpose of this paper is to provide a fully parameterized, multibody dynamics modeling and optimization approach for front-loading washing machines. Subsequently, a BO framework with different infill techniques is developed, and global BO is performed on the parametrized model for minimizing the maximum displacement to ultimately avoid possible collision of the tub and frame. Two case studies based on the model with 5 DVs and the fully parametrized model with 9 DVs were conducted, and a comparative analysis is undertaken to identify the best infill strategies for improved optimization performance. The major technical findings obtained from this study are listed below:

1. The front-loading washing machine studied in this paper was parameterized with nine DVs successfully that cover all critical suspension elements affecting the washing machine movement and are amenable to design optimization.
2. Our study indicates that the fully parametrized model with a total of nine DVs offers more room for design optimization, leading to the lower maximum displacement when compared to a model with a lower number of DVs.
3. Two types of acquisition function are examined in this study, and the comparison shows that optimization with Expected Improvement converges faster than Lower bound infill criterion.
4. Optimal values of the rotation speed and spring stiffness were close to the lower bounds given the specified range, which is within the expectation.
5. Optimal mass density and damping coefficient values occurred at upper bounds, aligning with the previous research findings [20] that higher damping coefficients reduce amplitudes, and higher mass density lowers amplitude.
6. Front and rear dampers' Z coordinates experienced significant fluctuations before reaching optimal values. Front and rear dampers' front angles underwent multiple variations but eventually reached optimal values in the BO process.
7. For the 9 DV case with EI criterion, dampers' angle fluctuations were more pronounced compared to the one with LB criterion.

In the future, several lines of effort can be pursued to further optimize the model or expand upon the research

findings. These may include construction of the washing machine, instrumentation and experimental setups to collect testing results for model validation, and development of new parameterizable models with different BO configurations for washing machines of other types.

**Acknowledgements** The research was funded by Samsung Electronics Co., LT and the South Carolina Department of Commerce. The opinions expressed in this article are solely those of the authors and do not represent the opinions of the sponsors.

**Funding** Open access funding provided by the Carolinas Consortium.

## Declarations

**Conflict of Interest** The corresponding author, on behalf of all the authors, affirms that no conflicts of interest are present.

**Open Access** This article is licensed under a Creative Commons Attribution 4.0 International License, which permits use, sharing, adaptation, distribution and reproduction in any medium or format, as long as you give appropriate credit to the original author(s) and the source, provide a link to the Creative Commons licence, and indicate if changes were made. The images or other third party material in this article are included in the article's Creative Commons licence, unless indicated otherwise in a credit line to the material. If material is not included in the article's Creative Commons licence and your intended use is not permitted by statutory regulation or exceeds the permitted use, you will need to obtain permission directly from the copyright holder. To view a copy of this licence, visit <http://creativecommons.org/licenses/by/4.0/>.

## References

- Boyraz P, Gündüz M (2013) Dynamic modeling of a horizontal washing machine and optimization of vibration characteristics using genetic algorithms. *Mechatronics* 23(6):581–593
- Chen HW, Zhang Q (2017) Design of horizontal axis washing machine with ball balancer and MR dampers. *Int J Precis Eng Manuf* 18(12):1783–1793
- Drach I, Goroshko A, Dwornicka R (2021) Design principles of horizontal drum machines with low vibration. *Adv Sci Technol Res J* 15(2):258–268
- Kimmel T, Kunkel C, Ait Sghir M, Kessler A (2023) Potential of ultrasonics for energy saving in the household washing process. *Energ Effic* 16(5):33
- Bui QD, Nguyen QH, Hoang LV, Mai DD (2021) A new self-adaptive magneto-rheological damper for washing machines. *Smart Mater Struct* 30(3):037001
- Kim HG, Nguyen TM, Lee G, Lim C, Wang S (2021) Efficient topography optimization of a washing machine cabinet to reduce radiated noise during the dehydration process. *J Mech Sci Technol* 35:973–978
- Sánchez-Tabuenca B, Galé C, Lladó J, Alberó C, Latre R (2020) Washing machine dynamic model to prevent tub collision during transient state. *Sensors* 20(22):6636
- Jeong JS, Sohn JH, Kim CJ, Park JH (2023) Dynamic analysis of top-loader washing machine with unbalance mass during dehydration and its validation. *J Mech Sci Technol* 37(4):1675–1684
- Jo MG, Kim JH, Choi JW (2020) Rebalancing method for a front-loading washing machine using a robot balancer system. *Int J Control Autom Syst* 18(4):1053–1060
- Jang JS, Jin JH, Jung HY, Park JH, Lee JW, Yoo WS (2016) Multi-body dynamic analysis of a washing machine with a rapid change of mass during dehydration. *Int J Precis Eng Manuf* 17(1):91–97
- Yağcı BC, Erol H (2015) Semiactive vibration control for horizontal axis washing machine. *Shock Vibr* 2015:692570
- Chen HW, Yuan XT, Sun Z, Mou QQ, Xiong M, Wang WH (2022) Design and analysis of an active balancing mechanism for a vertical axis washing machine. *Int J Precis Eng Manuf* 23(7):763–778
- Hong ZK, Chen YF (2014) Dynamic modeling and optimization on the automatic balancing of a washing machine. In: *Applied mechanics and materials*, vol 620. Trans Tech Publications Ltd, Bâch, pp 304–309
- Chen HW, Zhang QJ, Wu XQ (2015) Stability and dynamic analyses of a horizontal axis washing machine with a ball balancer. *Mech Mach Theory* 87:131–149
- Bracquené E, Peeters J, Alfieri F, Sanfelix J, Duflou J, Dewulf W, Cordella M (2021) Analysis of evaluation systems for product reparability: a case study for washing machines. *J Clean Prod* 281:125122
- Park J, Jeong S, Yoo H (2021) Dynamic modeling of a front-loading type washing machine and model reliability investigation. *Machines* 9(11):289
- Xiao L, Zhang S (2017) Analysis and optimization of drum washing machine vibration isolation system based on rigid-flexible virtual prototype model. *J Vibroeng* 19(3):1653–1664
- Nygårds T, Berbyuk V (2014) Optimization of washing machine kinematics, dynamics, and stability during spinning using a multistep approach. *Optim Eng* 15(2):401–442
- In D, Lim DG, Min J, Kim SW, Seo H, Kim S, Cheong C et al (2024) Robust design optimization of spin algorithm to reduce spinning time and vibration in washing machine. *AIP Adv* 14(3)
- Hashemian F, Deng X, Wang Y, Kim S, Vaidhyanathan R (2023) A comprehensive study of the effects of various design variables on the dynamic behavior and vibration characteristics of a front-loading washing machine. *Noise Vibr Worldwide* 54:477–491
- Shahriari B, Swersky K, Wang Z, Adams RP, De Freitas N (2015) Taking the human out of the loop: a review of Bayesian optimization. *Proc IEEE* 104(1):148–175
- Wang X, Jin Y, Schmitt S, Olhofer M (2023) Recent advances in Bayesian optimization. *ACM Comput Surv* 55(13s):1–36
- Ungredda J, Branke J (2021) Bayesian optimisation for constrained problems. *arXiv preprint arXiv:2105.13245*
- Frazier PI (2018) Bayesian optimization. In: *Recent advances in optimization and modeling of contemporary problems*. Informs, Seattle, WA, pp 255–278
- Xu X, Zhang Y (2023) A Gaussian process regression machine learning model for forecasting retail property prices with Bayesian optimizations and cross-validation. *Decis Anal J* 8:100267
- Nikolaidis P, Chatzis S (2021) Gaussian process-based Bayesian optimization for data-driven unit commitment. *Int J Electr Power Energy Syst* 130:106930
- Kamrah E, Ghoreishi SF, Ding ZJ, Chan J, Fuge M (2023) How diverse initial samples help and hurt Bayesian optimizers. *J Mech Des* 145(11):111703
- Zhang Z, Chen HC, Cheng QS (2020) Surrogate-assisted quasi-Newton enhanced global optimization of antennas based on a heuristic hypersphere sampling. *IEEE Trans Antennas Propag* 69(5):2993–2998
- Afzal A, Kim KY, Seo JW (2017) Effects of Latin hypercube sampling on surrogate modeling and optimization. *Int J Fluid Mach Syst* 10(3):240–253
- Akramin MRM, Ariffin AK, Kikuchi M, Abdullah S (2017) Sampling method in probabilistic S-version finite element analysis for initial flaw size. *J Braz Soc Mech Sci Eng* 39:357–365

31. Cozad A, Sahinidis NV, Miller DC (2014) Learning surrogate models for simulation-based optimization. *AIChE J* 60(6):2211–2227
32. Yang H, Hong SH, ZhG R, Wang Y (2020) Surrogate-based optimization with adaptive sampling for microfluidic concentration gradient generator design. *RSC Adv* 10(23):13799–13814
33. Parr JM, Keane AJ, Forrester AI, Holden CM (2012) Infill sampling criteria for surrogate-based optimization with constraint handling. *Eng Optim* 44(10):1147–1166
34. Sobester A, Forrester A, Keane A (2008) *Engineering design via surrogate modelling: a practical guide*. John Wiley & Sons
35. Albadr MA, Tiun S, Ayob M, Al-Dhief F (2020) Genetic algorithm based on natural selection theory for optimization problems. *Symmetry* 12(11):1758
36. Zainuddin FA, Abd Samad MF, Tunggal D (2020) A review of crossover methods and problem representation of genetic algorithm in recent engineering applications. *Int J Adv Sci Technol* 29(6s):759–769
37. Alam T, Qamar S, Dixit A, Benaida M (2020) Genetic algorithm: reviews, implementations, and applications. *arXiv preprint. arXiv:2007.12673*
38. Lambora A, Gupta K, Chopra K (2019) Genetic algorithm—a literature review. In: 2019 International conference on machine learning, big data, cloud and parallel computing (COMITCon). IEEE, Piscataway, NJ, pp 380–384

**Publisher's Note** Springer Nature remains neutral with regard to jurisdictional claims in published maps and institutional affiliations.